Solar Phys (2010) 266: 39–58
DOI 10.1007/s11207-010-9586-4

Multiwavelength Study of the M8.9/3B Solar Flare from AR NOAA 10960

Pankaj Kumar · A.K. Srivastava · B. Filippov · Wahab Uddin

Received: 9 December 2009 / Accepted: 27 May 2010 / Published online: 15 July 2010

Abstract We present a multiwavelength analysis of a long-duration, white-light solar flare (M8.9/3B) event that occurred on 04 June 2007 from AR NOAA 10960. The flare was observed by several spaceborne instruments, namely SOHO/MDI, *Hinode*/SOT, TRACE, and STEREO/SECCHI. The flare was initiated near a small, positive-polarity, satellite sunspot at the center of the active region, surrounded by opposite-polarity field regions. MDI images of the active region show a considerable amount of changes in the small positive-polarity sunspot of δ configuration during the flare event. SOT/G-band (4305 Å) images of the sunspot also suggest the rapid evolution of this positive-polarity sunspot with highly twisted penumbral filaments before the flare event, which were oriented in a counterclockwise direction. It shows the change in orientation, and also the remarkable disappearance of twisted penumbral filaments ($\approx 35-40\%$) and enhancement in umbral area ($\approx 45-50\%$) during the decay phase of the flare. TRACE and SECCHI observations reveal the successive activation of two helically-twisted structures associated with this sunspot, and the corresponding brightening in the chromosphere as observed by the time-sequence of SOT/Ca II H line (3968 Å) images. The secondary, helically-twisted structure is found to be associated with the M8.9 flare event. The brightening starts six – seven minutes prior to the flare maximum with the appearance of a secondary, helically-twisted structure. The flare intensity maximizes as the secondary, helically-twisted structure moves away from the active region. This twisted flux tube, associated with the flare triggering, did not launch a CME. The location of the flare activity is found to coincide with the activation site of the helically-twisted structures. We conclude that the activation of successive helical twists (especially the second

Electronic supplementary material The online version of this article (doi:10.1007/s11207-010-9586-4) contains supplementary material, which is available to authorized users.

P. Kumar (✉) · A.K. Srivastava · W. Uddin
Aryabhatta Research Institute of Observational Sciences (ARIES), Manora Peak, Nainital 263129, India
e-mail: pkumar@aries.res.in

B. Filippov
Pushkov Institute of Terrestrial Magnetism, Ionosphere and Radio Wave Propagation, Russian Academy of Sciences, Troitsk, Moscow Region 142190, Russia

one) in the magnetic-flux tubes/ropes plays a crucial role in the energy build-up process and the triggering of the M-class solar flare without a coronal mass ejection (CME).

Keywords Flares · Flux tubes · Magnetic fields · Corona

1. Introduction

Solar flares are sudden explosions in the solar atmosphere during which large amounts of the magnetic energy, stored in the twisted and sheared magnetic fields, is released by the process of magnetic reconnection in the form of thermal energy and particle acceleration. The flares associated with CME eruptions are known as "eruptive flares", while flares without association of CMEs are known as "confined flares". The emerging magnetic flux, rapid motion/rotation of sunspots, and interaction of filaments can destabilize the magnetic field and trigger solar eruptive phenomena, *e.g.*, flares, CMEs *etc.* (Min and Chae, 2009; Kumar, Manoharan, and Uddin, 2010). S-shaped or inverted S-shaped sigmoids indicate twisted field lines in the solar atmosphere. Solar eruptions usually take place due to the increase of the twist in the magnetic-field configurations of an active region (Canfield, Hudson, and McKenzie, 1999). Recently, the MHD models of magnetic-flux tubes show that twist $[\phi]$ of $2.5-3.5\pi$ is sufficient for solar eruptions, and the stable equilibrium of the magneto-fluid breaks when the total twist in the associated flux tubes exceeds this critical value (Fan and Gibson, 2003; Kliem, Titov, and Török, 2004; Török, Kliem, and Titov, 2004).

Nandy (2008) has discussed the formation, evolution, and ejection of magnetic-flux ropes, which originate in the twisted magnetic structures through the combined action of surface flux transport processes (such as diffusion, meridional circulation, and differential rotation). Ishii, Kurokawa, and Takeuchi (1998) have investigated a flaring active region [NOAA 5395] during March 1989 and found some peculiar vortex-like motion of small, satellite sunspots, which successively emerged from the leading edge of the sunspot group. They proposed a schematic model of successive emergence of twisted and winding magnetic-flux loops coiling around a trunk of magnetic-flux tube, and concluded the flare triggering was due to these emerging flux bundles. The twisted flux-tube model (Amari *et al.*, 2000) and flux-injection driven model (Krall *et al.*, 2001), both suggest that a twist-enhanced flux rope can play a crucial role in large-scale eruptive events. The primary mechanism for driving such eruptions may be due to the catastrophic loss of MHD equilibrium (Lin and Forbes, 2000). They suggested that a flux rope is allowed to escape with a fairly small reconnection rate in the vertical current sheet created below. The highly twisted flux tubes store magnetic energy, which is necessary for the heating and particle acceleration during the solar eruptions. Wang *et al.* (2002) found a rapid disappearance of a sunspot associated with the M2.4 flare from NOAA AR 9830 on 20 February 2002 with hard X-ray sources located near this disappeared sunspot. Ishii, Kurokawa, and Takeuchi (2000) have also pointed out that the occurrence of high flare activity is restricted to the location and the time at which the strongly twisted magnetic-flux ropes emerged into the photosphere in long-lived and large active regions, *e.g.*, NOAA AR 4201.

The observational evidences of twisted helical structure are less abundant in the solar atmosphere. However, they may be an efficient mechanism for the triggering of solar eruptive phenomena, *e.g.*, flares and coronal mass ejections (CMEs). Gary and Moore (2004) and Liu *et al.* (2003) have observed helical magnetic-flux tubes with multiple turns, which were associated with double flares and CMEs. This observational evidence of the activation of

helical flux tubes, and thus associated destabilization of large-scale magnetic fields of active region, may be important clues for the energy build-up processes of solar flares. However, we do not have sufficient understanding and observational signature of the twisted flux ropes and their evolution from the sub-photospheric level into the corona. There are a few observational signatures related to the generation of the twist in the solar filaments, which causes the disruption of their stable magnetic-field configuration and generates solar eruptive events (see, *e.g.*, Liu and Alexander, 2009; Williams *et al.*, 2005 and references cited there). Rust and LaBonte (2005) have also found evidence of sigmoids in the solar corona that were governed and energized by the magnetic twist, without any large-scale destabilization of magnetic fields and associated eruptions from the Sun. Gerrard, Arber, and Hood (2002) have found that the foot-point twisting motion may also generate the twisting in the active-region loops which trigger flare event after their reconnection with the surrounding opposite-polarity field lines.

AR 10960 shows successive activation of helically-twisted magnetic structures on 4 June 2007, which do not cause any eruption. Recently, evidence of the kink instability has been found in the right-handed twisted loop, which caused the B5.0 class flare in this AR during 04:40 – 04:51 UT (Srivastava *et al.*, 2010). In the present paper, we study the M8.9/3B flare of the same active region [NOAA 10960] during 05:06 – 05:16 UT on 4 June 2007 using multiwavelength observations. We find rare observational evidence of the activation of helically-twisted magnetic structure in the active region, which may produce the M-class flare. In Section 2, we present multiwavelength observations of AR 10960 and the associated flare. In later sections, we present the discussion and conclusions.

2. Multiwavelength Observations of NOAA 10960 and Associated M8.9/3B Flare

The flare was observed by various space-based instruments namely SOHO/MDI, *Hinode*/SOT, TRACE, and STEREO/SECCHI. The top panel of Figure 1 displays the SOHO/MDI image of the active region NOAA 10960 on 4 June 2007 before this flare activity. The active region is located near the eastern limb at S09E50 showing a $\beta\gamma\delta$ configuration. This active region produced ten M-class flares during its passage across the solar disk. However, this active region was very poor in CME production, and only two M-class flares were associated with CMEs (Yashiro, Gopalswamy, and Akiyama, 2008). In the present study, an M8.9/3B flare was triggered, without any CME eruption observed, on 4 June 2007. The positive-polarity sunspot, indicated by an arrow, plays an important role in triggering the M8.9/3B solar flare. The enlarged view of the sunspot group, as indicated by a box on SOHO/MDI image, is shown in the SOT/blue-continuum image (4504 Å) (bottom-left panel). A closer view of the positive-polarity sunspot, as indicated by a box in SOT/blue-continuum image, is also shown in the bottom-right panel. The penumbral filaments, twisted in the counterclockwise direction, are clearly evident in this image.

According to the GOES soft X-ray flux profiles in the 0.5 – 4 Å and 1 – 8 Å wavelength bands, the M8.9 flare starts at 05:06 UT, reaches maximum at 05:13 UT, and ends at 05:16 UT (Figure 9). This flare shows an impulsive rise for a short duration during the above-mentioned time period and then a gradual decay for a long time until nearly 06:45 UT. A small B5.0 class flare was also observed well before this flare during 04:40 – 04:51 UT, which seems to be a precursor for the M8.9 flare. According to Solar Geophysical Data (SGD), the M-class flare is classified as class 3B in Hα, where the flare starts at 05:05 UT, peaks at 05:14 UT and ends at 06:42 UT.

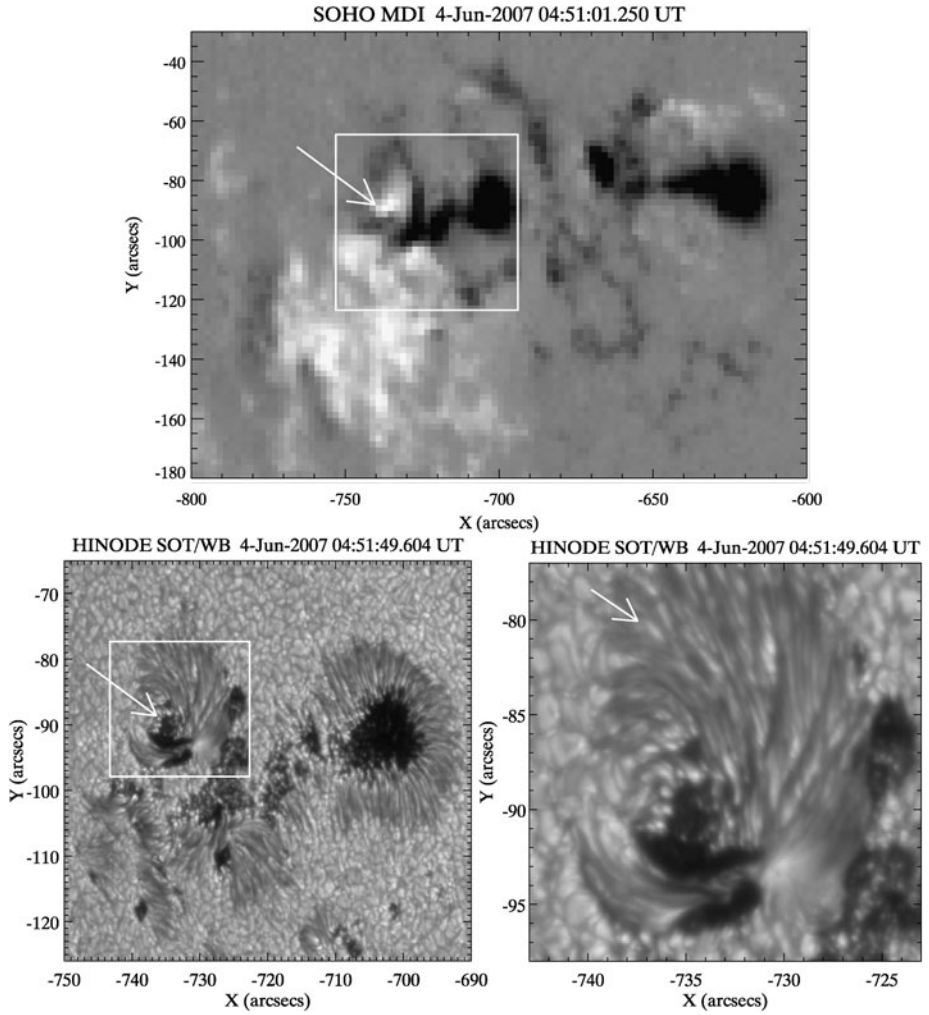

Figure 1 Top: SOHO/MDI image of active region NOAA 10960 on 04 June 2007. The positive-polarity sunspot indicated by arrow plays an important role in triggering the M8.9/3B solar flare. The enlarged view of the sunspot group of the active region as indicated by a box in SOHO/MDI image, is shown in the SOT/blue continuum (4504 Å) image (bottom-left panel). A closer view of the positive-polarity sunspot, as indicated by a box in the SOT/blue continuum image, is also shown in the bottom-right image. Penumbral filaments, twisted in the counterclockwise direction, are clearly evident in this image.

2.1. *Hinode*/SOT Observations

High-resolution filtergrams of the flaring region in NOAA 10960 were obtained by the 50-cm *Solar Optical Telescope* (SOT) onboard the *Hinode* spacecraft. We use the SOT/Ca II H 3968 Å chromospheric images at a cadence of ≈ one minute, with a spatial resolution of 0.1″ per pixel (Tsuneta *et al.*, 2008). We also use SOT/blue-continuum (4504 Å) temporal image data to examine the changes and evolution of the positive-polarity sunspot which is the key place at the center of the active region where the flare activity occurred. The *Hinode* data are calibrated and analyzed using standard IDL routines in the SolarSoft (SSW) package.

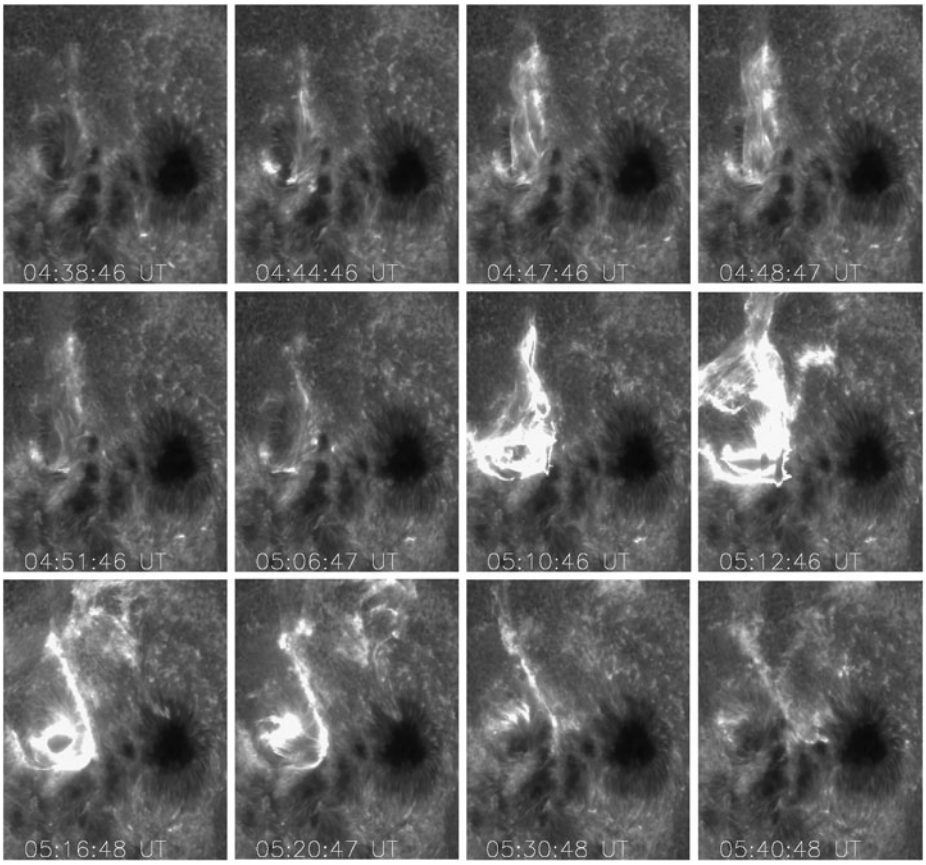

Figure 2 *Hinode*/SOT Ca II H 3968 Å images showing the successive activation of helical twists and corresponding brightening above the positive-polarity sunspot on 4 June 2007. Secondary helical twist was activated at ≈05:08 UT and causes the maximum of the M8.9/3B class flare brightening in the chromosphere at ≈05:13 UT. The size of each image is $60'' \times 75''$.

Figure 2 displays the selected chromospheric temporal images of the active region NOAA 10960 in Ca II H line. These images show significant changes in the chromosphere before the flare. The image at 04:42 UT shows two bright points at the two opposite edges of an umbral bridge structure. After that, a twisted, bright structure appears near the umbral bridge from the southern part of the sunspot. It is ≈29 000 km (in projection) from the sunspot location. This structure was visible for six – seven minutes (04:45 – 04:51 UT) and then it fades out against the chromosphere (Srivastava *et al.*, 2010).

After this first episode, two other bright points were observed at the same site before the initiation of the M8.9 flare (refer to the image at 05:06 UT). After this, the flare starts and it covers the entire sunspot at the maximum phase. The S-shaped single ribbon, formed at 05:16 UT, was observed until 05:26 UT. The flare continues until 05:30 UT. The twisted structure showed two successive activations at the same location, near the positive-polarity sunspot, in association with the energy build-up and release processes in AR 10960. It seems that the activation of secondary twist at ≈05:08 UT plays a significant role in the triggering of M8.9/3B solar flare.

2.2. TRACE and STEREO/SECCHI/EUVI Observations

We use TRACE 171 Å (Fe IX) EUV images to study the dynamics of the flaring active region and its response in the corona before the M-class flare event. This wavelength corresponds to 1.3 MK plasma. The image size is 1024 × 1024 pixels with resolution of 0.5″ per pixel, and the cadence is ≈ one minute. We have used the standard IDL routines available in the SolarSoft library for cleaning and co-aligning the images. Figure 3 displays the selected TRACE coronal images before the flare during 04:00 – 04:56 UT. A careful investigation of the TRACE movie shows the plasma flow from the flare site along the two close and smaller loops located within the big loop (see the image at 04:01:15 UT). The image at 04:39 UT shows a S-shaped sigmoid structure (indicated by an arrow) at the active-region center. At 04:43 UT, we observe two bright points near the sigmoid structure, which is also evident in SOT/Ca II temporal-image data. Therefore, the first helical twist has appeared in the loop system associated with this particular positive-polarity sunspot and also causes the brightening in the plasma there (see also the first panel of Figure 2). This sunspot is connected with the negative-polarity sunspot by very faint loop system in which the twist and brightening are activated, and their configuration is also highly variable (Srivastava *et al.*, 2010). The projected lower-bound speed of the activation of this twist is ≈ 200 km s^{-1}. It spreads to the maximum distance of ≈ 43 500 km from the sunspot (see the image at 04:48 UT). It was visible for nearly eight minutes. After that, the structure fades into the coronal background. TRACE observations of the activation of this primary helical twist correlate nicely with the SOT observations. However, the length of the structure is a little less in the SOT images in comparison to the TRACE observations. This is due to the smaller field of view of SOT (see the image at 04:48 UT in both sets), which only captured the partial extent of the helically-twisted loop system in the chromosphere. This structure, which is fully observed by TRACE, does not fit in the field of view of the SOT. However, TRACE missed the impulsive phase of this M-class flare. For the impulsive phase of the flare, we use the STEREO-A/SECCHI/EUVI observations (Wuelser *et al.*, 2004). We use Fe IX 171 Å coronal images for the present study. The size of each image is 2048 × 2048 pixels with 1.6″ per pixel sampling. We use the standard SECCHI_PREP subroutines for cleaning the images and other standard subroutines available in STEREO package SolarSoft library. We have used SOHO/MDI images for co-aligning the SECCHI images.

Figure 4 displays the selected SECCHI/EUVI coronal images during 05:03 – 05:56 UT. The image at 05:08 UT shows the secondary activation of helically-twisted structure above the same positive-polarity sunspot which connects the neighboring, small, negative-polarity sunspot (see the middle panel of Figure 5). It should be noted that the successive activation of the helical twists, at the same place that cause the plasma brightening also, may be a signature of the build-up of magnetic energy in AR 10960. However, the activation of the secondary helical twist at 05:08 UT seems to play a crucial role in the energy build-up process for the M8.9/3B class flare. This activation is located near the center of the active region where the flare initiation takes place, as it spreads away from the sunspot. The flare reaches maximum at ≈ 05:14 UT and then decays slowly. During the decay phase of the flare, the image at 05:23:30 UT shows a twisted flux rope (one turn is visible) very close to the flare energy-release site (indicated by an arrow). This structure moves away very slowly and finally disappears at 05:48 UT. However, during the maximum and decay phase of the flare, several twisted structures are visible, which indicate the presence of free magnetic energy in the observed coronal volume. We overlaid the MDI positive (red) and negative (blue) polarity contours over the selected SECCHI images to view the field morphology, during the flare event (see Figure 5). The careful investigation of these images reveals the

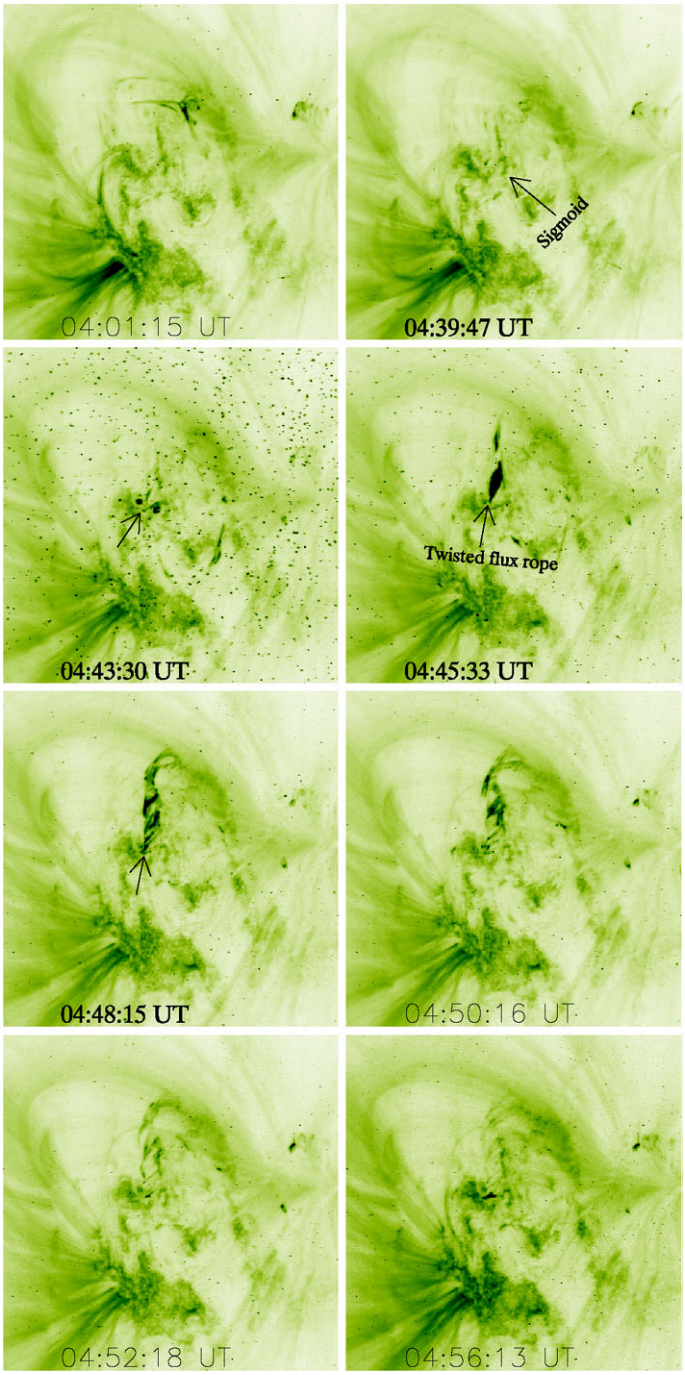

Figure 3 TRACE 171 Å EUV images (in reversed colors) showing the temporal changes in the magnetic-field configuration before the initiation of M-class flare. The size of each image is $200'' \times 200''$.

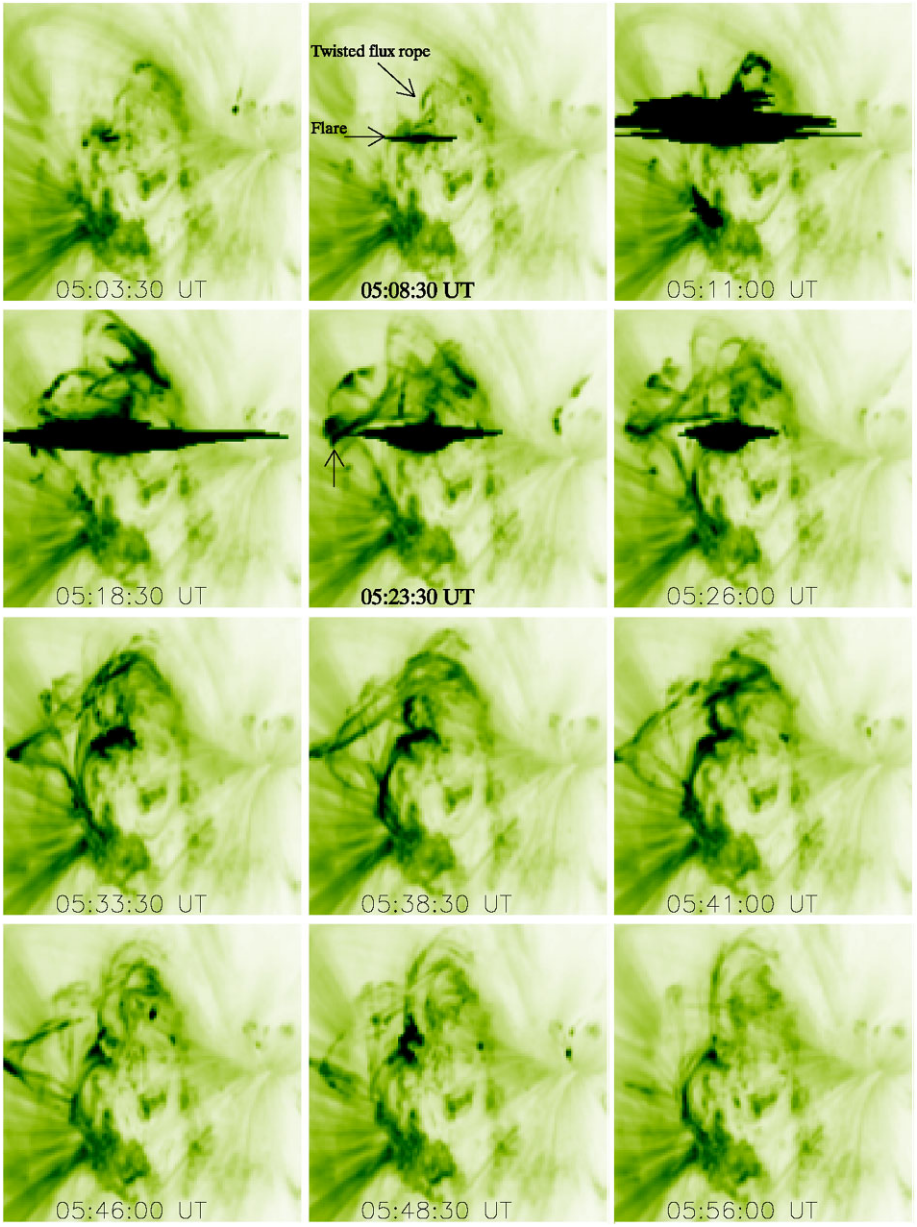

Figure 4 STEREO SECCHI 171 Å images (in reversed colors) showing the temporal changes in the magnetic-field configuration and related M8.9/3B flare event. The size of each image is $200'' \times 200''$.

association of secondary helically-twisted structure at 05:08 UT before the M-class flare maximum, associated with the small positive-polarity satellite sunspot. Activation of this twist is also clearly visible in SOT images. This structure seems to be moving to the North of the sunspot. The twist angle can be estimated by measuring the number of turns in the twisted helical structure. It is evident from STEREO/SECCHI images (see Figure 6) that the

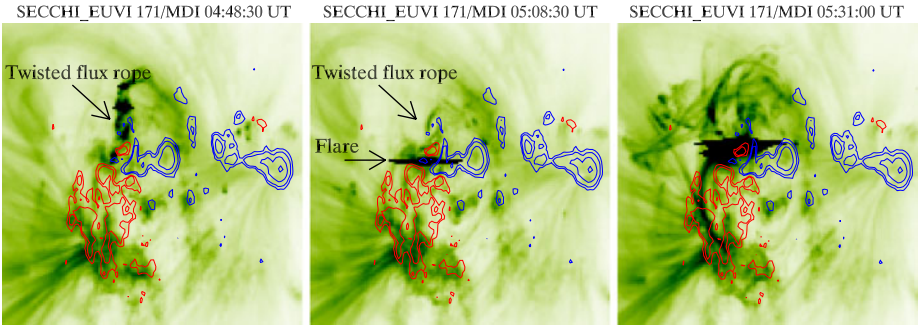

Figure 5 MDI contours overlaid on STEREO/SECCHI 171 Å EUV images before the flare initiation and during flare progressive phase. Red contours show positive polarity, while blue shows the negative polarity. The size of each image is $200'' \times 200''$.

secondary helically-twisted structure at 05:08 UT shows a minimum of two turns, suggesting that the total twist angle probably crosses the critical limit of 2.5π (the total twist angle is 4π). The flare brightening takes place in between a small positive and surrounding negative-polarity regions.

The rather small scale of the twisted coronal structures does not allow us to see differences in SECCHI/EUVI images of STEREO-A and STEREO-B spacecrafts with separation of only near 10° in June 2003 as is possible for more large-scale erupting structures (Gissot *et al.*, 2008; Liewer *et al.*, 2009). Figure 6 shows enlarged images of the twisted structure obtained by both STEREO-A and -B spacecraft. The upper parts of the helix are aligned with visible coronal loops, while the bottom parts are assumed to keep the same pitch angle. According to this assumption, some two turns of the helix can be recognized especially within the secondary twisted structure (bottom panel of Figure 6). In fact it looks like a multiple-thread screw and it is difficult to follow one particular thread through the whole flux-rope length. Approximate conservation of the pitch angle can help to estimate the amount of the total twist. The primary helical twist occurred during 04:42 – 04:51 UT, given in the upper panel for comparison with the secondary helically-twisted structure. The primary helical twist presented here for comparison is found to be the triggering mechanism of the B5.0 class flare during 04:40 – 04:51 UT (Srivastava *et al.*, 2010).

3. Sunspot Evolution in SOHO/MDI and SOT/G Band Images

We use SOHO/MDI observations to see the magnetic-field evolution during the flare. The size of each image is 1024×1024 ($2''$ per pixel resolution) with a cadence of 96 minutes (Scherrer *et al.*, 1995). We use the standard SolarSoft library to correct the differential rotation and analyze the magnetograms. Figure 7 displays the sequence of MDI images on 03 and 04 June 2007. The MDI time-sequence images reveal the interesting features, which show the considerable changes (area enhancement) in the positive-polarity sunspot during the decay phase of M-class flare event. Figure 8 displays the selected SOT/G-band images which show the partial field of view of the active region containing the same positive-polarity sunspot as marked by an arrow. This sunspot also shown by the red contour in Figure 5, which is associated with successive activation of the helical twists. The evolution of the small positive-polarity sunspot initially shows the highly twisted penumbral filaments in

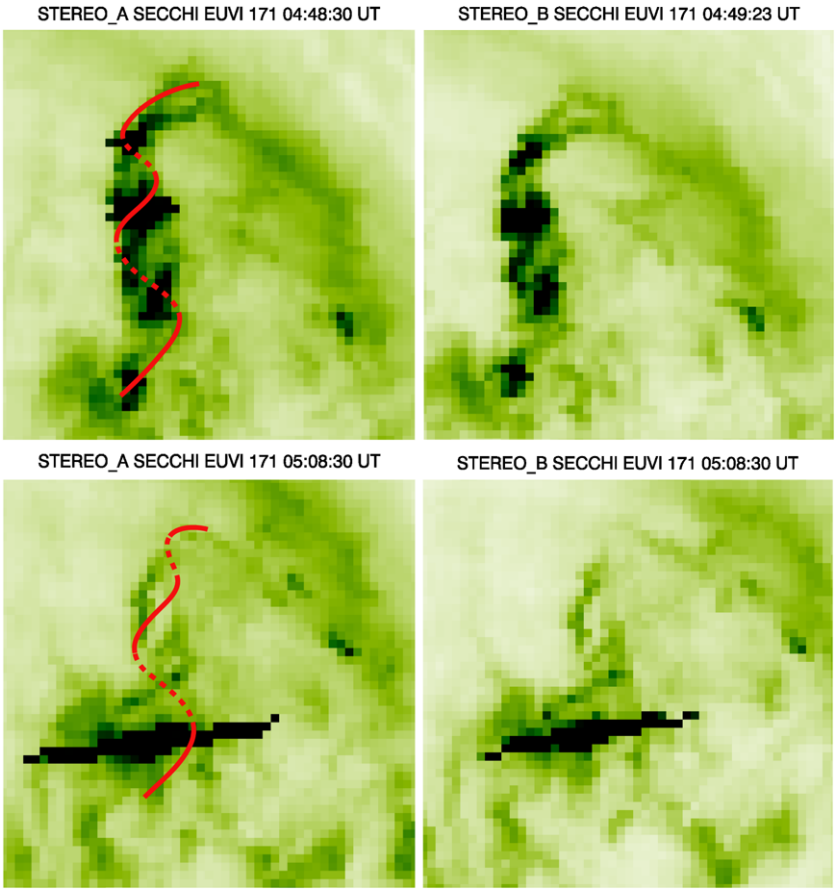

Figure 6 STEREO/SECCHI A and B images of the twisted helical structure. The secondary helical twist with approximately two turns (indicated by red line) has been activated on 05:08 UT just before the maximum of M8.9/3B class flare (bottom panel). The top-left panel shows, for the comparison, three turns (indicated by red line) during the activation of the first helical twist as estimated by Srivastava *et al.* (2010). The size of each image is $80'' \times 80''$.

the counterclockwise direction (*i.e.* sunspot rotation is clockwise) well before the flare (indicated by an arrow) as the active region lies in the southern hemisphere. This secondary twist at the footpoint of the loop system associated with this sunspot may be responsible for the energy build-up process of M-class flare occurred in this active region. The brightening (two bright points) takes place at the opposite edges of the umbral part of this sunspot. Then, a secondary twisted helical structure rises up from the same site (Section 2.1). The image observed at 05:12 UT shows the white-light flare at the sunspot (indicated by arrow) during its impulsive phase. During the decay phase of the M-class flare, we notice several changes in the sunspot: *i*) disappearance of twisted penumbral filaments in the northern part of the sunspot (indicated by boxes), *ii*) orientation change in the sunspot (shown by dotted line). Before the initiation of the flare activity, the sunspot shows a spherical shape with counterclockwise penumbral filaments, whereas after the flare activity it shows an elongated shape with penumbral changes (*i.e.* decay of penumbral filaments). We have estimated the projected height (elongation) *vs.* time profile of the twisted magnetic structures observed

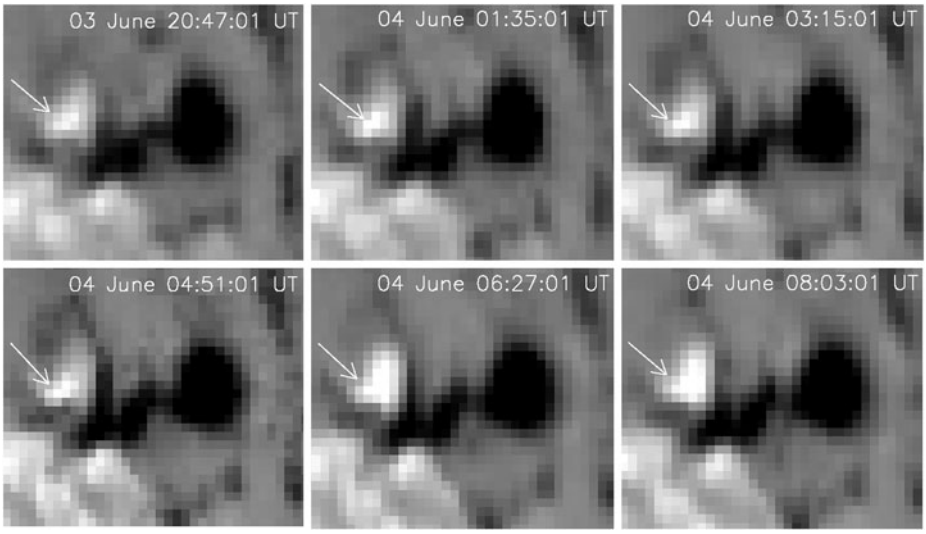

Figure 7 The selected SOHO/MDI images of the flare site. The arrow indicates the evolution of positive magnetic-flux region before and after the flare activity. The size of each image is $70'' \times 60''$.

in TRACE and SECCHI measurements, following the apex of the structure from the center of the active region and plotted against soft X-ray flux measurements (Figure 9, top). It is evident from the plot that the flare is closely associated with the activation and rising motion of the twisted magnetic structures/flux ropes. The co-temporal enhancement of the GOES soft X-ray flux profile with the increase of the projected height of the primary helical structure validate the findings of Srivastava *et al.* (2010) that this twist was probably responsible for B5.0 class flare. While again the co-temporal enhancement of the soft X-ray flux profile with the increase of the height of the secondary, helically-twisted structure shows its association with the M8.9/3B flare event that occurred in AR 10960. We have used the SOT/blue-continuum (4504 Å) images for quantitative estimation of penumbral and umbral changes during the flare event. We selected a box of $16'' \times 22''$ covering the sunspot of δ configuration. We extracted the total counts less than 700 for umbral change and between 700 – 1400 for penumbral changes. For viewing the change in area of both umbra and penumbra, we draw the umbral and penumbral boundaries using standard routines in IDL libraries and then extracted the total number of umbral and penumbral pixels of the sunspot. Figure 9 displays the temporal changes in umbral and penumbral intensity and area with respect to the soft X-ray flux profile. It is evident from the figure that there are remarkable changes in the umbral and penumbral structures. However, the rapid change in umbral portion at $\approx$05:12 UT is due to the flare that covers the sunspot umbra. After the flare maximum, we observe considerable penumbral disappearance ($\approx 35 - 40\%$) and enhancement ($\approx 45 - 50\%$) in the umbral area. This enhancement of the positive-polarity spot is evident in the SOHO/MDI magnetograms during the decay phase of the M-class flare (see Figure 7). This suggests that the magnetic field becomes more vertical from the initial horizontal configuration, which is in agreement with the previous studies (Wang *et al.*, 2004; Liu *et al.*, 2005). These changes suggest the loss of magnetic energy with sunspot evolution and that energy seems to be released in the form of flare thermal energy.

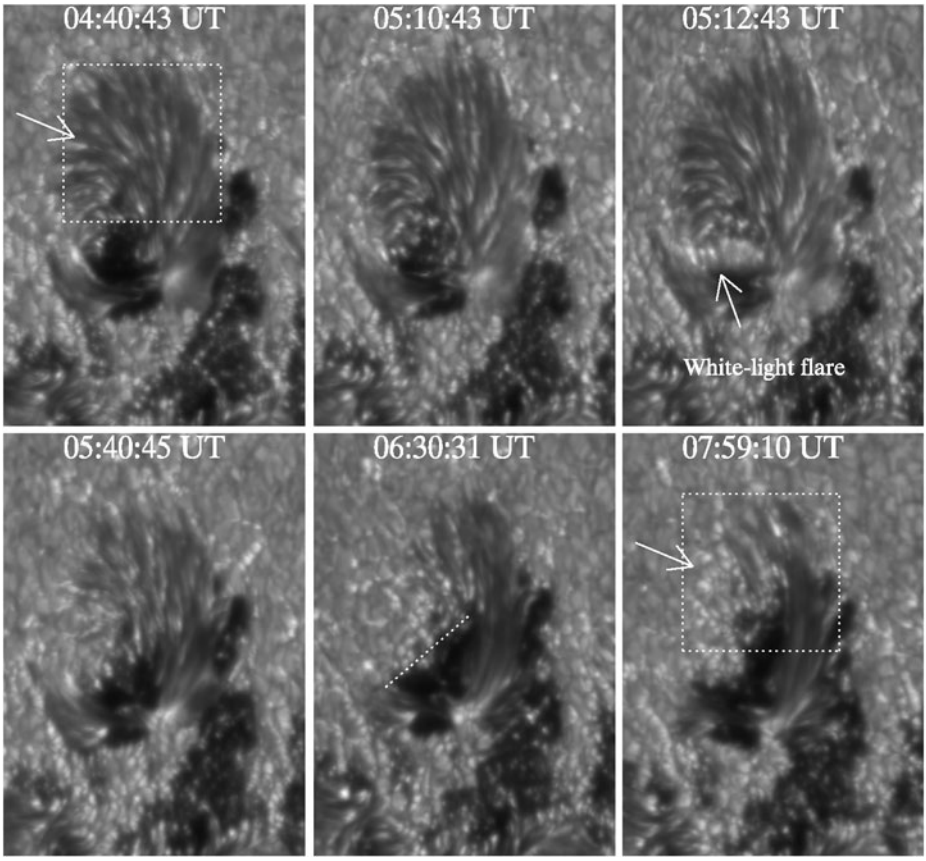

Figure 8 The selected SOT/G-band images (4305 Å) showing the evolution of the positive-polarity sunspot (before, during and after the M8.9/3B class flare). The dotted line and boxes reveal the orientation change and disappearance of twisted penumbral filaments respectively after the flare. The size of each image is $25'' \times 35''$.

4. Discussion

We study the M8.9/3B flare event on 4 June 2007 from NOAA AR 10960 using multiwavelength observations. It is shown that the small positive-polarity sunspot plays an important role in triggering this flare event, which lies at the center of the active region and it is associated with the twisted flux tube/rope where successive helical twists have been activated before the flare event. MDI observations also reveal a considerable amount of enhancement in the area of the positive-polarity sunspot at the flare site during the decay phase of the M-class flare which is in agreement with the SOT/G-band observations. Another interesting point is that the positive-polarity sunspot seems to be highly sheared (*i.e.* twisted penumbral filaments) before the flare activity. During the decay phase and after the flare event, the sunspot indicates major changes in its structure. It shows twisted penumbral filament disappearance in the northern part of the sunspot. Before the flare, the penumbral structure was highly sheared showing anticlockwise orientation. After the flare, it becomes more simplified with the loss of some area. This suggests the loss of twisted magnetic energy associated with the sunspot, which may be released in the form of flare thermal energy.

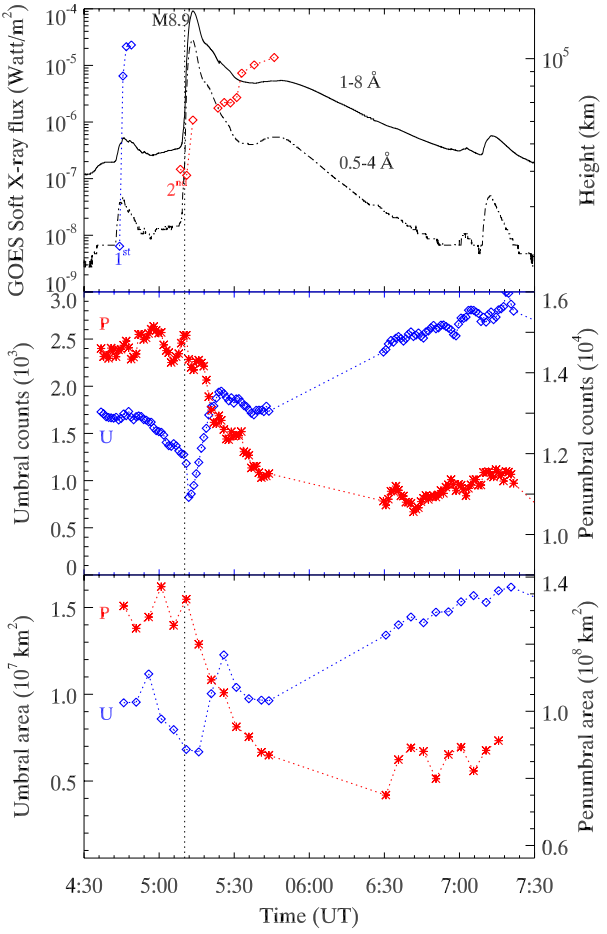

Figure 9 Top: Projected height (elongation) *vs.* time profiles of both twisting helical magnetic structures with soft X-ray flux profiles of the flares on 4 June 2007. This plot clearly indicates that the rise of magnetic structures is closely associated with the flare onset. Middle and bottom: Umbral and penumbral changes (indicated by "U" and "P" respectively) in intensity and area to show the link with soft X-ray flux profiles. It is evident from the plot that there are remarkable changes (umbral enhancement and penumbral decay) in both umbra and penumbra after the flare maximum.

For investigating the overlying magnetic-field environment of this active region, we have used the potential-field source surface (PFSS) extrapolation (Altschuler and Newkirk, 1969; Schatten, Wilcox, and Ness, 1969) before the flare event at 00:04 UT (see Figure 10). We rotate the SOHO/MDI image for our convenience to see the morphology of the magnetic field. The active region lies near the eastern limb during that time. The coronal magnetic-field topology is on average in agreement with TRACE and SECCHI observations.

Figure 11 shows a schematic scenario of the event, which we have deduced from the multiwavelength analysis. EUV images reveal several flux tubes that seem to play a major role in the progress of the flaring activity. There are large loops that straddle the whole active region. They connect the southern border of the large area of positive-polarity and small fragments of negative-polarity to the North of the major sunspots. Two smaller flux tubes originate from the vicinities of the foot-points of the large loop but end at the center of the active region. The northern flux tube connects with the positive-polarity sunspot, while the southern flux tube connects with the negative-polarity magnetic flux concentrations nearby the sunspot. There is also a short flux tube connecting the dominant, positive polarity of the sunspot with the small portion of its umbra with opposite polarity. The highly twisted structure of the sunspot penumbra indicates the presence of the twist within the short flux tube

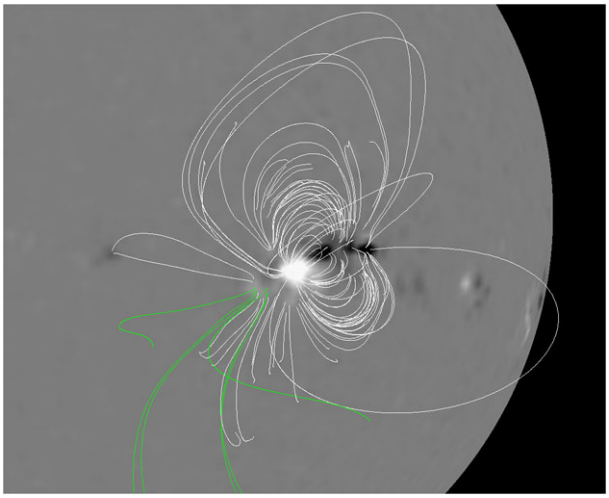

Figure 10 Potential-field source surface (PFSS) extrapolation of the NOAA AR 10960 at 00:04 UT on 4 June 2007. White lines show the closed magnetic fields whereas green lines show the open fields.

and the northern flux tube. The most clear twisting of the northern flux tube becomes visible after its activation. The character of the brightening propagation allows us to conclude that the twist within the northern flux tube does not appear during the flare, but existed long before the flare. Therefore, the positive-polarity sunspot is the footpoint of the flux rope. Some part of this magnetic-flux tube/rope is connected with distant photospheric negative elements and some part is connected with the negative portion of the same umbra. After the activation, caused possibly by the emergence of new magnetic flux which manifests itself in our region of interest as a growth of the area of positive polarity (Figure 7), several field lines of the flux rope may reconnect with the field lines of the southern flux tube. As a result, a new, long flux tube is created as well as short loops that connect the former central footpoints of reconnecting field lines (Figure 11(b)). This short loop corresponds to the post-flare loop system visible in SOT/Ca II H line images. Reconnected, long field lines move up and the twist propagates from the flux rope along the whole length of the flux tube. The field lines form a loop firstly or a noose (Figure 11(c)), and then make up a wide tangled structure (Figure 11(d)). It is most likely that the presence of the twist causes the field lines to move up, however they stop at some higher altitude. Therefore, the whole scenario may also resemble a failed flux-rope eruption (Filippov and Koutchmy, 2002; Ji *et al.*, 2003). After the flare, the magnetic-field configuration becomes simplified. There is no longer a clear manifestation of the twisted magnetic field. Field lines of the positive-polarity sunspot become more connected to the nearby negative polarities to the West of the sunspot. This possibly results in disappearance of penumbral filaments in the northeast part of the sunspot.

SOT and TRACE observations indicate the successive activation of helical, twisted flux bundles just above the same positive-polarity sunspot (at the edges of the twisted umbral structure) well before the flare. As the secondary activation of the helical twist rises at 05:08 UT, the M-class flare intensity maximizes. This can be interpreted as the rising of twisted flux rope and its progressive reconnection with the surrounding opposite-polarity field region. The plasma is heated up, evaporated, and pumped into the two smaller loops (underlying a major loop system), which connect to the reconnection site with opposite magnetic polarities (refer to the SECCHI images during the decay phase of the flare).

Srivastava *et al.* (2010) have observed the first activation of a highly (right-handed) twisted flux tube in AR 10960 during the period 04:43 – 04:52 UT. They have estimated

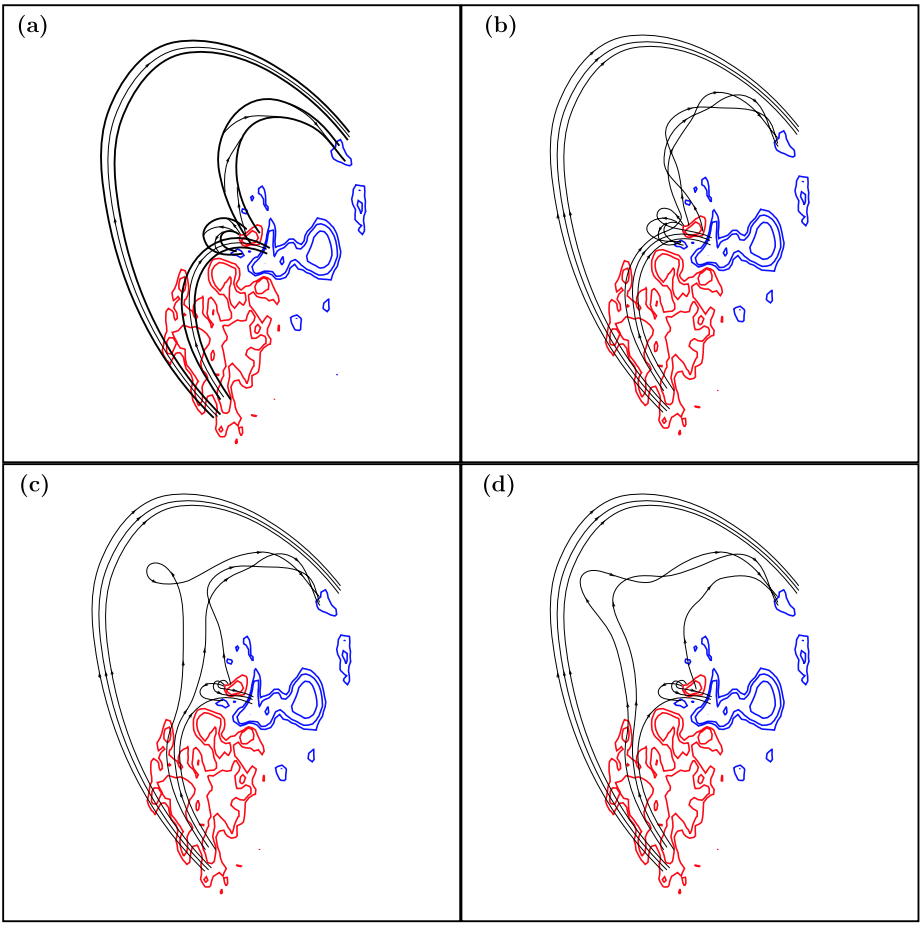

Figure 11 Schematic demonstrating the magnetic configuration of the active region before and during the flare. Red contours show the positive-polarity sunspots whereas blue indicate the negative-polarity sunspots.

the length and the radius of the loop as $L \approx 80$ Mm and $a \approx 4.0$ Mm respectively, and also estimated the total maximum twist angle as $\Phi \approx 12\pi$, by assuming quasi-symmetric distribution of the twist over the magnetic loop, which is much larger than the Kruskal – Shafranov instability criterion. They have found that right-handed twist may be asymmetrically distributed over the observed loop, which is smoothed with the Alfvénic time ≈ 80 seconds and possess a quasi-symmetric maximum twist. The detection of a clear double structure of the loop top during 04:47 – 04:51 UT in TRACE 171 Å images are found to be consistent with simulated kink instability in curved coronal loops (Török, Kliem, and Titov, 2004). They have suggested that the kink instability of this twisted magnetic loop triggered the B5.0 class solar flare, which also occurred between 04:40 – 04:51 UT in this active region. The co-spatial brightening in soft X-rays as observed by *Hinode*/XRT and the co-temporal occurrence of the right-handed twisting in the flux tube confirm the occurrence of the B5.0 flare during 04:40 – 04:51 UT probably due to the generation of the kink instability. We have also found the secondary twist of the same handedness (right-handed) in the magnetic-flux tube at the same place as in the STEREO images at 05:08 UT (refer to Figure 6). Therefore,

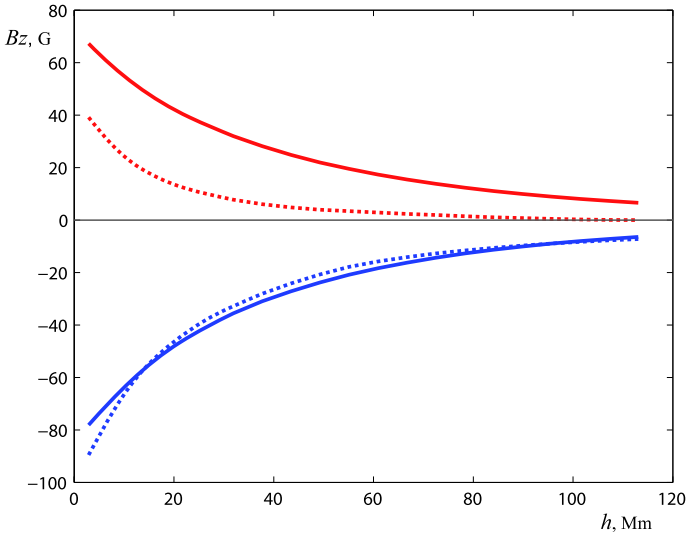

Figure 12 Dependence of the average vertical magnetic field at different heights for the active regions NOAA 10501 (dotted curves) and NOAA 10960 (thick curves). Red and blue curves correspond respectively to positive and negative magnetic-field strength.

the activation of a second helical twist may also be associated with the kink instability in the active region which may trigger the M-class flare on 05:08 UT. In Figure 6, we present the twisted flux tube observed by TRACE, STEREO-A and -B. We find the activation of the secondary twist on the observed loop with same right-handedness and ≈two turns in the flux tube (*i.e.* $\approx 4\pi$ twist) at first halve of the loop (see bottom panel of Figure 6). This is also crossing the threshold of minimum twist for the stability in the flux tube.

Ishii, Kurokawa, and Takeuchi (1998) also have reported that the flare-productive magnetic shear is produced by the emergence of twisted magnetic-flux bundle. Magnetic energy is stored in the twisted flux bundle, which is originally formed in the convection zone and released as flares in the course of the emergence of the twisted flux bundle above the photosphere. Our study provides the most likely signature of the successive activation of the helical twist in the flux tubes/ropes moving away from the active region. The location of the flare activity coincides with the area of the positive magnetic flux increase. Therefore, it may be concluded that the magnetic energy stored in the helically-twisted flux bundles is released as a flare by reconnecting with the surrounding opposite-polarity field lines, when it moves away from AR. This active region produced an M-class flare without any coronal mass ejections (CMEs) on 4 June 2007. According to analytical and numerical models of magnetic flux-rope eruption, the behavior of the flux rope strongly depends on the rate of ambient magnetic-field decrease with height (van Tend and Kuperus, 1978; Forbes and Priest, 1995; Török, Kliem, and Titov, 2004; Török and Kliem, 2005). If the magnetic field is strong enough at high altitude and has a significant horizontal component, the ascending motion of a flux rope can be stopped at a greater height and does not lead to formation of a CME. We compared the coronal potential magnetic field of NOAA AR 10960 with the magnetic field of NOAA AR 10501 studied by Kumar, Manoharan, and Uddin (2010), which produced a fast full-halo CME. Figure 12 shows the averaged vertical magnetic field $[B_z]$ as a function of height $[h]$ for both active regions. The area of about 220 × 240 Mm from MDI magnetograms was used as a boundary condition

for numerically solving the Neumann external boundary-value problem (Schmidt, 1964; Filippov and Den, 2001). Magnetograms on 19 November 2003 and 7 June 2007 were chosen for the dates when the active regions were close to the center of the solar disk. The 220×240 Mm area covers all marked photospheric magnetic fields of the active regions. Positive and negative magnetic flux were calculated at different heights and then divided by the area occupied by this flux to obtain magnetic flux density or averaged magnetic-field strength. The dependence of average vertical magnetic field at different heights for the NOAA AR 10501 (dotted curves) and NOAA AR 10960 (thick curves) is compared in Figure 12 in which red and blue curves respectively correspond to the positive and negative magnetic-field strength.

It is evident that magnetic field in the CME-productive AR falls more rapidly with height than in the other one and the magnetic flux is unbalanced. Positive flux is negligible above 30 Mm, which is evidence of weak horizontal field needed to retard the flux rope's ascending motion. In contrast, positive and negative fluxes in NOAA AR 10960 are nearly equal and decrease slowly and synchronously with height. This means a large-scale, closed magnetic field that is present and able to support the flux-rope equilibrium at high altitude. As was stressed by Török and Kliem (2005), the decrease of the overlying field with height is a main factor in deciding whether kink instability leads to a confined event or to a CME.

Therefore, large-scale destabilization of AR 10960 magnetic fields does not occur during this flare. Our multiwavelength and high-resolution observational results from recent space-borne instruments reveal the dynamics of this active region and the associated M-class flare, which may be unique evidence for further theoretical modeling and observational studies of those active regions that produce solar flares but are the poor originators of CMEs. This observational evidence may also be useful in the forecasting of the occurrence of large-scale solar eruptive phenomena from similar kinds of active regions. However, further statistical, multiwavelength studies should be carried out using forthcoming high-resolution space and ground-based observations to investigate the dynamics and mechanism respectively for multiple active regions and associated flares, which do not produce any large-scale CMEs. These studies may be useful to find the detailed physical scenario and dynamics of such active regions.

5. Conclusions

We find multiwavelength evidence of the successive activation of helical twists that may help in the energy build-up process at the flare site. The energy is released later in the form of an M-class flare after secondary activation of this critical twist in the flux tube/rope and its reconnection with neighboring opposite fields. The main conclusions of this study may be summarized as follows:

i) We report the dynamics of a single, positive-polarity sunspot having twisted penumbral filament structure and successive activation of twisted helical magnetic structures.

ii) The activation of two helical structures/ropes played an important role in destabilizing the field lines and in triggering the flare. The twist in the secondary magnetic structures crosses the threshold $(2.5 - 3.5\pi)$, which probably produces the kink instability in this structure. The energy-release site of the M-class flare at the center of the active region coincides with the activated twisted magnetic structures. Ishii, Kurokawa, and Takeuchi (1998) pointed out that the successive emergence of helical flux bundles plays a crucial role in triggering flares and showed it by a schematic; here we provide the observational evidence of the scenario.

iii) The M-class flare shows agreement with the quadrupolar (closed – closed) reconnection model (breakout) between two closed field lines (Antiochos, 1998). The asymmetric evolution is driven by foot-point shearing of one side of an arcade, where reconnection between the sheared arcade and the neighboring (unsheared) flux system triggers the flare. As the twisted magnetic structure moves away from the reconnection site, the flare intensity increases and reaches maximum. This reveals the progressive reconnection of the twisted magnetic structure with the surrounding opposite-polarity fields.

iv) Penumbral disappearance during the decay phase and after of the flare suggests that the magnetic-field structure becomes more vertical. This indicates that the magnetic field changes from a highly inclined to an almost vertical configuration during the decay phase of the flare (just after the flare maximum), *i.e.* part of the penumbral magnetic field is converted into umbral fields. Our results are in agreement with previous studies (Wang *et al.*, 2004; Liu *et al.*, 2005).

v) The decrease of the overlying field with height is a main factor in deciding whether the kink instability leads to a confined event or to a CME (Török and Kliem, 2005). In AR 10960, the slow variation of vertical component of the magnetic field with height is found to be the most likely cause for the failed eruption during M-class flare.

Acknowledgements We thank the reviewers for their valuable suggestions, which improved the manuscript considerably. We acknowledge SOHO/MDI and TRACE for providing the data used in this study. SOHO is a project of international cooperation between ESA and NASA. We acknowledge the *Hinode* and STEREO missions for providing us the high-resolution data. *Hinode* is a Japanese mission developed and launched by ISAS/JAXA, with NAOJ as domestic partner and NASA and STFC (UK) as international partners. It is operated by these agencies in cooperation with ESA and NSC (Norway). This work was supported in part by the Department of Science and Technology, Ministry of Science and Technology of India and in part by the Russian foundation for Basic Research (grants 09-02-00080 and 09-02-92626, INT/RFBR/P-38). We also express our gratitude to the editor Prof. John Leibacher for his editorial corrections which improved the manuscript considerably.

References

Altschuler, M.D., Newkirk, G.: 1969, Magnetic fields and the structure of the solar corona. I: Methods of calculating coronal fields. *Solar Phys.* **9**, 131 – 149. doi:10.1007/BF00145734.

Amari, T., Luciani, J.F., Mikic, Z., Linker, J.: 2000, A twisted flux rope model for coronal mass ejections and two-ribbon flares. *Astrophys. J. Lett.* **529**, L49 – L52. doi:10.1086/312444.

Antiochos, S.K.: 1998, The magnetic topology of solar eruptions. *Astrophys. J. Lett.* **502**, L181 – L184. doi:10.1086/311507.

Canfield, R.C., Hudson, H.S., McKenzie, D.E.: 1999, Sigmoidal morphology and eruptive solar activity. *Geophys. Res. Lett.* **26**, 627 – 630. doi:10.1029/1999GL900105.

Fan, Y., Gibson, S.E.: 2003, The emergence of a twisted magnetic flux tube into a preexisting coronal arcade. *Astrophys. J. Lett.* **589**, L105 – L108. doi:10.1086/375834.

Filippov, B.P., Den, O.G.: 2001, A critical height of quiescent prominences before eruption. *J. Geophys. Res.* **106**, 25177 – 25184. doi:10.1029/2000JA004002.

Filippov, B., Koutchmy, S.: 2002, About the prominence heating mechanisms during its eruptive phase. *Solar Phys.* **208**, 283 – 295.

Forbes, T.G., Priest, E.R.: 1995, Photospheric magnetic field evolution and eruptive flares. *Astrophys. J.* **446**, 377 – 389. doi:10.1086/175797.

Gary, G.A., Moore, R.L.: 2004, Eruption of a multiple-turn helical magnetic flux tube in a large flare: evidence for external and internal reconnection that fits the breakout model of solar magnetic eruptions. *Astrophys. J.* **611**, 545 – 556. doi:10.1086/422132.

Gerrard, C.L., Arber, T.D., Hood, A.W.: 2002, The triggering of MHD instabilities through photospheric footpoint motions. *Astron. Astrophys.* **387**, 687 – 699. doi:10.1051/0004-6361:20020491.

Gissot, S.F., Hochedez, J., Chainais, P., Antoine, J.: 2008, 3D reconstruction from SECCHI-EUVI images using an optical-flow algorithm: method description and observation of an erupting filament. *Solar Phys.* **252**, 397 – 408. doi:10.1007/s11207-008-9270-0.

Ishii, T.T., Kurokawa, H., Takeuchi, T.T.: 1998, Emergence of a twisted magnetic flux bundle as a source of strong flare activity. *Astrophys. J.* **499**, 898 – 904. doi:10.1086/305669.

Ishii, T.T., Kurokawa, H., Takeuchi, T.T.: 2000, Emergence of twisted magnetic-flux bundles and flare activity in a large active region, NOAA 4201. *Publ. Astron. Soc. Japan* **52**, 337 – 354.

Ji, H., Wang, H., Schmahl, E.J., Moon, Y., Jiang, Y.: 2003, Observations of the failed eruption of a filament. *Astrophys. J. Lett.* **595**, L135 – L138. doi:10.1086/378178.

Kliem, B., Titov, V.S., Török, T.: 2004, Formation of current sheets and sigmoidal structure by the kink instability of a magnetic loop. *Astron. Astrophys.* **413**, L23 – L26. doi:10.1051/0004-6361:20031690.

Krall, J., Chen, J., Duffin, R.T., Howard, R.A., Thompson, B.J.: 2001, Erupting solar magnetic flux ropes: theory and observation. *Astrophys. J.* **562**, 1045 – 1057. doi:10.1086/323844.

Kumar, P., Manoharan, P.K., Uddin, W.: 2010, Evolution of solar magnetic field and associated multi-wavelength phenomena: flare events on 20 November 2003. *Astrophys. J.* **710**, 1195 – 1204. doi:10.1088/0004-637X/710/2/1195.

Liewer, P.C., de Jong, E.M., Hall, J.R., Howard, R.A., Thompson, W.T., Culhane, J.L., Bone, L., van Driel-Gesztelyi, L.: 2009, Stereoscopic analysis of the 19 May 2007 erupting filament. *Solar Phys.* **256**, 57 – 72. doi:10.1007/s11207-009-9363-4.

Lin, J., Forbes, T.G.: 2000, Effects of reconnection on the coronal mass ejection process. *J. Geophys. Res.* **105**, 2375 – 2392. doi:10.1029/1999JA900477.

Liu, R., Alexander, D.: 2009, Hard X-ray emission in kinking filaments. *Astrophys. J.* **697**, 999 – 1009. doi:10.1088/0004-637X/697/2/999.

Liu, Y., Jiang, Y., Ji, H., Zhang, H., Wang, H.: 2003, Observational evidence of a magnetic flux rope eruption associated with the X3 flare on 2002 July 15. *Astrophys. J. Lett.* **593**, L137 – L140. doi:10.1086/378284.

Liu, C., Deng, N., Liu, Y., Falconer, D., Goode, P.R., Denker, C., Wang, H.: 2005, Rapid change of δ spot structure associated with seven major flares. *Astrophys. J.* **622**, 722 – 736. doi:10.1086/427868.

Min, S., Chae, J.: 2009, The rotating sunspot in AR 10930. *Solar Phys.* **258**, 203 – 217. doi:10.1007/s11207-009-9425-7.

Nandy, D.: 2008, Magnetic helicity, coronal heating and solar flaring activity: a review of the role of active region twist. In: Howe, R., Komm, R.W., Balasubramaniam, K.S., Petrie, G.J.D. (eds.) *Subsurface and Atmospheric Influences on Solar Activity* **CS-383**, Astron. Soc. Pac., San Francisco, 201 – 212.

Rust, D.M., LaBonte, B.J.: 2005, Observational evidence of the kink instability in solar filament eruptions and sigmoids. *Astrophys. J. Lett.* **622**, L69 – L72. doi:10.1086/429379.

Schatten, K.H., Wilcox, J.M., Ness, N.F.: 1969, A model of interplanetary and coronal magnetic fields. *Solar Phys.* **6**, 442 – 455. doi:10.1007/BF00146478.

Scherrer, P.H., Bogart, R.S., Bush, R.I., Hoeksema, J.T., Kosovichev, A.G., Schou, J., Rosenberg, W., Springer, L., Tarbell, T.D., Title, A., Wolfson, C.J., Zayer, I., MDI Engineering Team: 1995, The solar oscillations investigation – Michelson Doppler imager. *Solar Phys.* **162**, 129 – 188. doi:10.1007/BF00733429.

Schmidt, H.U.: 1964, On the observable effects of magnetic energy storage and release connected with solar flares. In: Hess, W.N. (ed.) *NASA Spec. Publ.* **50**, 107.

Srivastava, A.K., Zaqarashvili, T.V., Kumar, P., Khodachenko, M.L.: 2010, Observation of kink instability during small B5.0 solar flare on 2007 June 4. *Astrophys. J.* **715**, 292 – 299. doi:10.1088/0004-637X/715/1/292.

Török, T., Kliem, B.: 2005, Confined and ejective eruptions of kink-unstable flux ropes. *Astrophys. J. Lett.* **630**, L97 – L100. doi:10.1086/462412.

Török, T., Kliem, B., Titov, V.S.: 2004, Ideal kink instability of a magnetic loop equilibrium. *Astron. Astrophys.* **413**, L27 – L30. doi:10.1051/0004-6361:20031691.

Tsuneta, S., Ichimoto, K., Katsukawa, Y., Nagata, S., Otsubo, M., Shimizu, T., Suematsu, Y., Nakagiri, M., Noguchi, M., Tarbell, T., Title, A., Shine, R., Rosenberg, W., Hoffmann, C., Jurcevich, B., Kushner, G., Levay, M., Lites, B., Elmore, D., Matsushita, T., Kawaguchi, N., Saito, H., Mikami, I., Hill, L.D., Owens, J.K.: 2008, The solar optical telescope for the *Hinode* mission: an overview. *Solar Phys.* **249**, 167 – 196. doi:10.1007/s11207-008-9174-z.

van Tend, W., Kuperus, M.: 1978, The development of coronal electric current systems in active regions and their relation to filaments and flares. *Solar Phys.* **59**, 115 – 127. doi:10.1007/BF00154935.

Wang, H., Ji, H., Schmahl, E.J., Qiu, J., Liu, C., Deng, N.: 2002, Sudden disappearance of a small sunspot associated with the 2002 February 20 M2.4 flare. *Astrophys. J. Lett.* **580**, L177 – L180. doi:10.1086/345713.

Wang, H., Liu, C., Qiu, J., Deng, N., Goode, P.R., Denker, C.: 2004, Rapid penumbral decay following three X-class solar flares. *Astrophys. J. Lett.* **601**, L195 – L198. doi:10.1086/382188.

Williams, D.R., Török, T., Démoulin, P., van Driel-Gesztelyi, L., Kliem, B.: 2005, Eruption of a kink-unstable filament in NOAA active region 10696. *Astrophys. J. Lett.* **628**, L163 – L166. doi:10.1086/432910.

Wuelser, J., Lemen, J.R., Tarbell, T.D., Wolfson, C.J., Cannon, J.C., Carpenter, B.A., Duncan, D.W., Gradwohl, G.S., Meyer, S.B., Moore, A.S., Navarro, R.L., Pearson, J.D., Rossi, G.R., Springer, L.A., Howard, R.A., Moses, J.D., Newmark, J.S., Delaboudiniere, J., Artzner, G.E., Auchere, F., Bougnet, M., Bouyries, P., Bridou, F., Clotaire, J., Colas, G., Delmotte, F., Jerome, A., Lamare, M., Mercier, R., Mullot, M., Ravet, M., Song, X., Bothmer, V., Deutsch, W.: 2004, EUVI: the STEREO-SECCHI extreme ultraviolet imager. In: Fineschi, S., Gummin, M.A. (eds.) *SPIE* **CS-5170**, 111 – 122. doi:10.1117/12.506877.

Yashiro, S., Gopalswamy, N., Akiyama, S.: 2008, Poor CME productivity in active region 10960. AGU Spring Meeting Abstracts, A3.